Risk Evaluation of Hybrid Microgrids Considering DC-Link Voltage Stability

Azizi, Ali; Peyghami, Saeed; Wang, Huai; Blaabjerg, Frede

Published in:
Proceedings of the 2022 IEEE 13th International Symposium on Power Electronics for Distributed Generation Systems (PEDG)

DOI (link to publication from Publisher):
10.1109/PEDG54999.2022.9923273

Publication date:
2022

Document Version
Accepted author manuscript, peer reviewed version

A New Risk Assessment Approach for Design of Hybrid Microgrids Considering Stability Issues

Ali Azizi *, Frede Blaabjerg, Saeed Peyghami

Energy Department, Aalborg University, 9220 Aalborg East, Aalborg, Denmark

*aaz@energy.aau.dk

Abstract: Stability issues can significantly increase the risk of hybrid microgrids (HMGs), particularly during island mode operation. The dynamic performance of the system can induce constraints and stability margins that may elevate the loss of load probability. This paper presents a new stability-oriented risk assessment model that bridges the conventional reliability models, stability, and system risk. The proposed model ensures the risk of the system by considering the redesign or reconfiguration of HMGs to address stability issues. Firstly, the interlinking converters (ICs) DC-link voltage stability is analysed to determine the acceptable power flow margins in rectifying and inversion mode. Next, the new general risk assessment model is introduced. The results show that the stability margin significantly increases the risk of the HMG, particularly when considering the aging of converters. The study also examines the impact of various load characteristics and ICs with different numbers but the same total size. In some cases, the risk is acceptable for the desired loads, or it can be reduced to an admissible level by reconfiguring the ICs. Finally, the paper demonstrates the effectiveness of the proposed model in the optimal design of HMGs, aiming to guarantee the system's risk.

1. Introduction

Hybrid microgrids (HMGs) have emerged as a crucial component in power electronic-based systems, capable of functioning in both grid-connected and off-grid modes [1]. However, their small scale, high integration of renewables, and lower inertia present distinctive challenges, particularly when operating in island mode [2]. Key concerns encompass reliability, stability, power quality, and resiliency [3]. Maintaining a delicate balance between generation and load is imperative for microgrid operation, necessitating a system that is both reliable and stable, ensuring an uninterrupted power supply within an acceptable risk threshold. Stability and reliability, affecting both dynamic and static performance, are of paramount significance.

In contrast to conventional power systems, microgrids employ power electronics for energy conversion. With the increasing utilization of power electronics, susceptibility to load loss becomes a potential risk [4]. Load loss can stem from two primary factors: static and dynamic performance. While static performance pertains to component failures and is integrated into traditional reliability assessment models [5], dynamic performance directly influences system stability [6]. Nevertheless, transients and stability issues related to voltage/frequency in microgrids can escalate system risk without causing component failure [7, 8]. In these scenarios, microgrid components may face limitations due to over/under voltage/frequency issues or DC-link voltage instability of power converters. Thus, considering the intertwined nature of reliability and stability and their collective impact on overall system risk is essential for robust risk assessment methods.

Reliability concerns can also exert an influence on HMG stability. For instance, the aging of power converter components like switches and capacitors can induce voltage fluctuations potentially leading to system instability [9]. Furthermore, power converter aging can trigger various instability issues, such as thermal instability [10], frequency instability [11], and harmonic distortion [12]. These intricate connections between reliability and stability, coupled with heightened system risk, may substantially shape power converter design.

Current risk assessment methodologies predominantly concentrate on identifying static failures originating from components [13]. These models ascertain potential failure modes, evaluating the probability and consequences of each. Typically, risk assessment in power electronic-based systems operates at three levels [14]. At the component level, the reliability of individual components such as capacitors and switches are analyzed [15, 16]. Factors like mission profiles [18], temperature [19], humidity [20], and vibration [21] significantly impact component reliability and, consequently, system risk. System-level evaluation scrutinizes the overall system reliability using various risk techniques like failure modes and effects analysis [22], fault tree analysis [23], and event tree analysis [24]. Components are modeled in series or parallel configurations with respect to reliability, aiming to meet the desired standard of reliability [4]. At the operational level, the system's reliability throughout its lifespan is assessed, encompassing maintenance, repair, and replacement [25]. At this stage, the system's availability is monitored, and if it falls below the minimum risk threshold, redesigning may be necessary from the component level up [14]. However, these models solely consider component failure, and system reliability is predicated on static performance. In microgrids, where components are highly interdependent, susceptibility to stability issues that may destabilize the entire system and result in greater load loss is elevated. Consequently, this form of dynamic failure elevates

the overall system risk.

The stability challenges and classification in microgrids can be bifurcated into two primary categories: (1) control system stability and (2) power supply and balance stability [26]. The transients and dynamics resulting from this classification may have distinct impacts on system risk. For example, in the HMG structure depicted in Fig. 1, interlinking converters (ICs) play a pivotal role in ensuring system stability. As demonstrated in [27-29], the DC-link voltage of the ICs may operate in an unstable state during rectifying mode. This instability stems from the non-minimum phase characteristic, a consequence of the ac-filter inductance, which restricts power flow during rectification, heightening the likelihood of load loss in HMGs. Additionally, inappropriate control strategies, particularly in island mode, may induce frequency stability challenges [30, 31]. The impact of imprecise tuning of droop gains in microgrids with droop control has been explored in [32], revealing that excessive gains lead to significant frequency fluctuations even with minor load changes. Conversely, reducing gains diminishes the system's responsiveness to load alterations. Consequently, in hybrid microgrids, minor disturbances can upset the balance between load and frequency, increasing risk.

The conventional approach has separately addressed stability and reliability issues in modern power electronic-based systems, without considering the interplay between static and dynamic failures in risk assessment models. However, this interplay is indispensable for designing systems that are both stable and reliable. Enhancing risk assessment models necessitates accounting for how static and dynamic failures interact and their potential influence on overall system reliability. This will lead to a more comprehensive understanding of potential risks and more effective measures to prevent failures, ensuring the secure and reliable operation of power systems.

To tackle these challenges, this paper proposes a novel stability-oriented approach for risk assessment in power electronic-based power systems. This approach aims to model both static and dynamic system performance, establishing a direct link between system risk, stability, and reliability for HMGs. By doing so, it becomes possible to optimize the converter design to ensure the stability and reliability of the power grid. This new approach holds the potential to enhance the accuracy of risk assessment models and enable more effective management of potential risks associated with modern power systems.

The subsequent sections of this paper are organized as follows: Section 2 delves into the analysis of interlinking converter DC-link voltage stability to derive stability constraints for use in the ensuing sections. Section 3 introduces the proposed stability-oriented risk assessment model for hybrid microgrids, elucidating how it bridges stability and reliability. Section 4 presents various simulations and case studies demonstrating the capability of the proposed model in designing HMGs for stable and reliable operation. Finally, Section 5 provides important insights and a summary of the paper's outcomes.

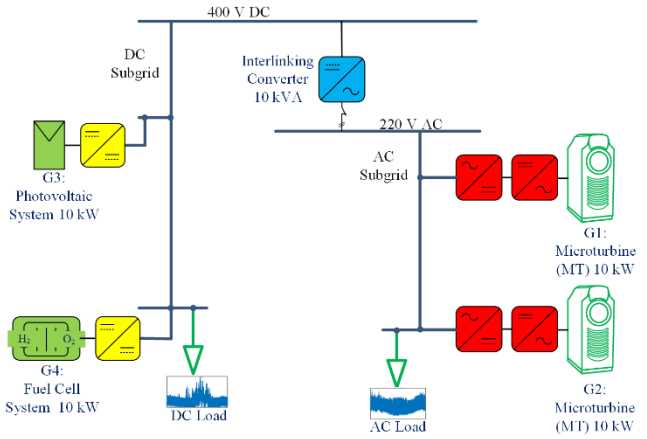

Fig. 1. *Single line diagram of a hybrid microgrid with one interlinking converter between ac and dc subgrids*

2. DC-link Voltage Stability of Interlinking Converters

Stability issues in microgrids are distinct from those found in conventional power systems due to their small size, strong coupling between system variables, low inertia, among other factors [33]. Based on the PES TR66 classification, stability challenges in microgrids arise from control system, power supply, and balancing issues [26]. Thus, there are numerous stability concerns that can impact the risk of microgrids. As it is not feasible to examine all of these issues in a single study, this paper focuses on analyzing DC-link voltage stability to validate the proposed model.

Fig. 2 presents a comprehensive depiction of the IC's architecture and control mechanism, which links the dc sub-grid to the ac sub-grid. Depending on the power status of distributed generators (DGs) and loads, the IC can transfer power in both inversion and rectifying modes, requiring the IC to be stable in both operating modes. A precise nonlinear model of the IC has been investigated in prior studies [30, 31]. The following section describes the mathematical model of the IC to determine the minimum required stability margin to ensure a stable IC operation. The power balance equation of the IC can be derived using (1) [30].

$$\frac{1}{2}C_{dc}\frac{d}{dt}(V_{dc}^2) = P_{dc} - P_{ac} \quad (1)$$

The first term of (1) represents the energy stored in the dc-link capacitor (C_{dc}) with V_{dc} denoting the voltage across the capacitor. P_{dc} and P_{ac} are the exchanged dc and ac powers, respectively, as shown in Fig. 2. Due to the nonlinearity of the power balance equation with respect to V_{dc}, the energy stored in the capacitor (W) can be used as a state space variable, as shown in (2).

$$\frac{dW}{dt} = P_{dc} - P_{ac} \quad (2)$$

Conventional models usually overlook the stored energy (W_L) in the ac-side filter (L_f) as it has a small value compared to the other variables and is zero in steady-state operation. These models express the ac-side power as given in (3).

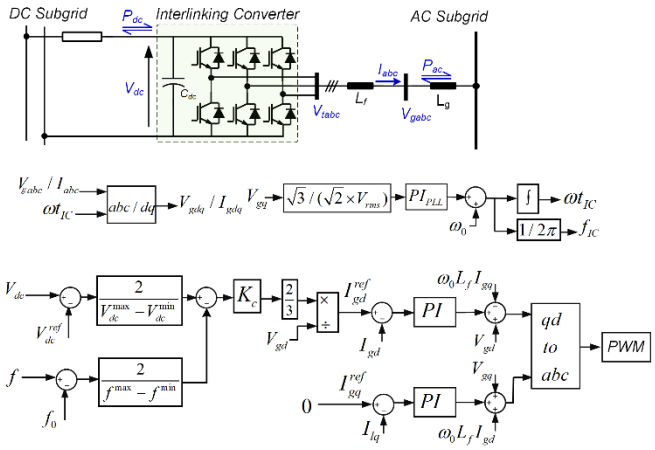

Fig. 2. *Structure of Interlinking Converter and control method*

$$P_{ac} = \frac{3}{2}\left(V_{gd}.I_{gd} + V_{gq}.I_{gq}\right) \tag{3}$$

where I_{gdq} and V_{gdq} are dq-frame components of the ac-side currents (I_{abc}) and voltages (V_{gabc}). However, this assumption may induce stability issues in certain operating points and degrade the stability margin. Hence, to address this issue, the P_{ac} can be rewritten as follows:

$$P_{ac} = \frac{3}{2}\left(V_{gd}.I_{gd} + V_{gq}.I_{gq}\right) + \frac{dW_L}{dt} \tag{4}$$

The term dW_L/dt is the instantaneous power of the ac filter and can be derived as (5) [30].

$$\begin{aligned} W_L &= \frac{3}{4}L_f\left(I_{gd}^2 + I_{gq}^2\right) \\ dW_L/dt &= \frac{3}{2}L_f\left(I_{gd}.\frac{dI_{gd}}{dt} + I_{gq}.\frac{dI_{gq}}{dt}\right) \end{aligned} \tag{5}$$

By substituting (4) and (5) into (2), it results in (6).

$$\begin{aligned} \frac{dW}{dt} = P_{dc} &- \frac{3}{2}V_{gd}I_{gd} - \frac{3}{2}V_{gq}I_{gq} \\ &- \frac{3}{2}L_f\left(I_{gd}\frac{dI_{gd}}{dt} + I_{gq}\frac{dI_{gq}}{dt}\right) \end{aligned} \tag{6}$$

The operation and control principle of the HMG is shown in Fig. 2. Notably, the power flow between ac and dc sub-grids has been performed using the normalized droop method, that is used for simulations and analysis the impact of uncertainties from ac and dc loads. The normalized dc voltage (V_{pu}) and the frequency (f_{pu}) can be obtained using (7) and (8) [33]. Normalization is necessary to coordinate the dc voltage and ac frequency.

$$V_{pu} = \frac{2}{V_{dc}^{max} - V_{dc}^{min}}\left(V_{dc} - V_{dc}^{ref}\right) \tag{7}$$

$$f_{pu} = \frac{2}{f^{max} - f^{min}}\left(f - f_0\right) \tag{8}$$

The minimum and maximum values of dc voltage and frequency are denoted by $V_{dc}^{min}/V_{dc}^{max}$ and f^{min}/f^{max} respectively, while V_{dc}^{ref}/V_{dc} and f_0/f represent the reference/operating values.

The reference current (I_{gd}^{ref}) of the IC can be achieved as:

$$I_{gd}^{ref} = \frac{2}{3V_{gd}}K_c.\left(V_{pu} - f_{pu}\right) \tag{9}$$

In (9) K_c is the droop gain and determines the portion of transferred power through the IC. It is worth mentioning that equation (9) is a general formulation. If the HMG is equipped with a single IC, the PI controller must be employed instead of the proportional gain K_c. However, when multiple ICs are in use, only K_c should be utilized to have stable operation.

The ac-side reactive power also can be calculated using (10):

$$Q_{ac} = \frac{3}{2}\left(V_{gd}.I_{gq} - V_{gq}.I_{gd}\right) \tag{10}$$

By considering the zero value for V_{gq}, according to (6) and (10) the dc-link voltage and reactive power can be controlled by I_{gd} and I_{gq}, respectively. This allows for the derivation of the control inputs V_{td} and V_{tq} are derived using (11) and (12).

$$\begin{aligned} V_{td} = V_{gd} - \omega_0 L_f I_{gd} + \left(k_p + k_I\int dt\right).(I_{gd}^{ref} \\ - I_{gd}) \end{aligned} \tag{11}$$

$$\begin{aligned} V_{tq} = V_{gq} + \omega_0 L_f I_{gq} + \left(k_p + k_I\int dt\right).(I_{gq}^{ref} \\ - I_{gq}) \end{aligned} \tag{12}$$

The ac voltage frequency (ω_{IC}) of the IC is extracted using a PLL and hence, the state equation of the PLL can be obtained as (13).

$$\frac{d\omega_{IC}}{dt} = \omega_0 + k_{p,PLL}.V_{gq}^{pu} + k_{I,PLL}.\int V_{gq}^{pu}\,dt \tag{13}$$

As mentioned above, the dynamic modeling in conventional models is simplified to (3), and a stable system operation can be achieved by using an appropriate PI controller. However, it will be shown that the ac-filter instantaneous power can lead to instability in the dc-link voltage loop in certain situations. Therefore, the impact of this power cannot be ignored.

The equation (6) can be linearized at the operating point as (14):

$$\frac{dW}{dt} = P_{dc} - \frac{3}{2}V_{gd}I_{gd} - \frac{3}{2}L_f\left(I_{gd}^0\frac{dI_{gd}}{dt} + I_{gq}^0\frac{dI_{gq}}{dt}\right) \tag{14}$$

Where V_{gq} is assumed to be zero by the PLL operation and (I_{gd}^0,I_{gq}^0) represent the operating point currents.

The I_{gd}^0 can be substituted by P_{dc} using (1) and (4) and considering the zero value for ac-filter power in steady state operation. Hence, I_{gd}^0 is obtained as $I_{gd}^0 = P_{dc}/1.5V_{gd}$.

Employing the Laplace transform in (14) and substituting I_{gd}^0 results (15), where "s" is the Laplace operator.

$$\begin{aligned} W(s) = \frac{P_{dc}(s)}{s} - \frac{\left(\frac{3}{2}V_{gd} + \frac{L_f P_{dc}}{V_{gd}}s\right)}{s}I_{gd}(s) \\ - \frac{3}{2}L_f I_{gq}^0 s I_{gq}(s) \end{aligned} \tag{15}$$

Equation (15) demonstrates that taking into account the dynamics of the ac-side filter results in a "zero" in the transfer function of $W(s)/I_{gd}(s)$, as shown in (16).

$$Z = -1.5V_{gd}^2/L_f P_{dc} \tag{16}$$

The location of the "zero" is dependent on P_{dc} changes

according to the mode of operation and the value of P_{dc}. In the inversion mode, where P_{dc} is positive, the "zero" appears on the left-hand side, resulting in a stable condition. On the contrary, in the rectifying mode, where P_{dc} is negative, the system will have a Right Half-Plane Zero (RHPZ). In such case, the system dynamics will be derived as nonminimum phase, and consequently the phase margin will be reduced if the value of P_{dc} is close to the IC rated capacity.

To demonstrate the impact of AC-filter dynamics and the resulting "zero" in the transfer function, an eigenvalue analysis was conducted. The IC and control system parameters are provided in Table 2 in the appendices. Fig. 3 illustrates the movement of the root locus of the dominant eigenvalues by varying P_{dc}. According to Fig. 3, when P_{dc} is increased in the inversion mode (dc to ac power flow), the dominant modes move towards the left-side of the S-plane. Therefore, the system will be stable due to higher damping.

Conversely, in the rectifying mode of operation, an increase in P_{dc} leads to movement of dominant modes towards the right half-plane and puts the system into an unstable condition. For instance, when the transferred power reaches to $P_{dc} = -0.93\,pu$, the dominant modes become very close to the origin, and the system becomes unstable thereafter. Hence, it is crucial to operate the IC within a limited boundary in terms of stability to avoid instability. The stability margin affects the risk of the HMG and increases the loss of load. Therefore, it is necessary to consider the impact of such stability issues in the risk assessment models.

3. Proposed Stability-Oriented Risk Assessment Approach

In this section, a new risk assessment method considering the stability issues for HMGs is proposed. This method simultaneously analyses the static and dynamic performance of the system, as illustrated in Fig. 4. The green frame represents the conventional risk assessment method, which focuses on the system's static performance. The blue frame indicates the proposed risk model, which bridges the dynamic performance stemming from stability issues and the conventional static performance. In the following, both methods are discussed.

3.1. Conventional Method

In conventional risk assessment methods for power systems, as depicted in Fig. 4, the availability state is generated based on the failure data of each component using various risk assessment techniques, such as Monte Carlo simulations [35], Markov chain [36], and also AI approaches [37]. Subsequently, the power availability of power generations (e.g., PV, Wind, Fuel Cell) is determined by convolving the availability states with the power mission profiles. These mission profiles may exhibit substantial fluctuations, as seen in PV and Wind units, or vary around a constant value.

In the next step, the power flow in HMGs is performed, adhering to the predetermined energy and power management strategies. The specific energy management method employed in this paper is discussed in section 4.3. Ultimately, the total risk of the system will be determined based on load losses. Various risk indices can be utilized to evaluate the

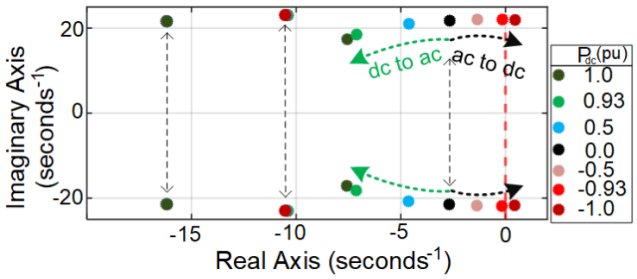

Fig. 3. *Impact of P_{dc} variation on loci of dominant modes*

frequency, duration, and amount of unsupplied loads [14]. In this study, regarding to the size of the HMG, two significant indices, namely, Loss of Load Expectation (LOLE) and Loss of Load Frequency (LOLF) are selected as the risk metrics. The mathematical representations of these indices are given in (17) [38].

$$LOLE = \frac{1}{N}.\sum_{i=1}^{N} LLD_i \quad \left(\frac{hr}{year}\right)$$
$$LOLF = \frac{1}{N}.\sum_{i=1}^{N} LLO_i \quad \left(\frac{occ}{year}\right) \tag{17}$$

Where N represents the number of sampling years, LLD_i represents the duration of load loss, and LLO_i is the loss of load occurrence.

Typically, these indices assess the system's overall risk, taking into account the components' static failure.

3.2. Proposed Method

To integrate the impact of dynamic performance into the overall system risk, the effect of stability can be represented as illustrated in Fig. 4. The IEEE PES technical report 66 provides guidance on incorporating various stability issues in HMGs. Once the stability issues in the HMG have been identified, the causes of instability can be determined using Root Cause Analysis (RCA) techniques such as eigenvalue analysis, root locus analysis, and time-domain simulations. Thus, for each stability issue, several stability margins and constraints are derived.

In the subsequent phase, the availability status of the relevant components affected by the identified instability issue is adjusted. This is achieved by combining the stability margins/constraints with the availability state generator models. For instance, in this study, as explained in section 2, the IC stability margin (Sm=0.93) is integrated with the IC availability state. As a result, the margins of the IC availability state shift from [-10, 10] kVA to [-9.3, 10] kVA. This implies that to ensure stable IC operation, the IC transferred power in rectifying mode should not exceed -9.3 kVA.

After modifying the availability states of the components, the updated availability states can be incorporated into the power unit's convolution and/or conventional energy management approach. Subsequently, new risk indices are generated that encompass both the dynamic and static failures of the HMG.

Thus, the proposed model bridges the stability and reliability, enabling a precise assessment of the system's overall risk, considering both static and dynamic failures.

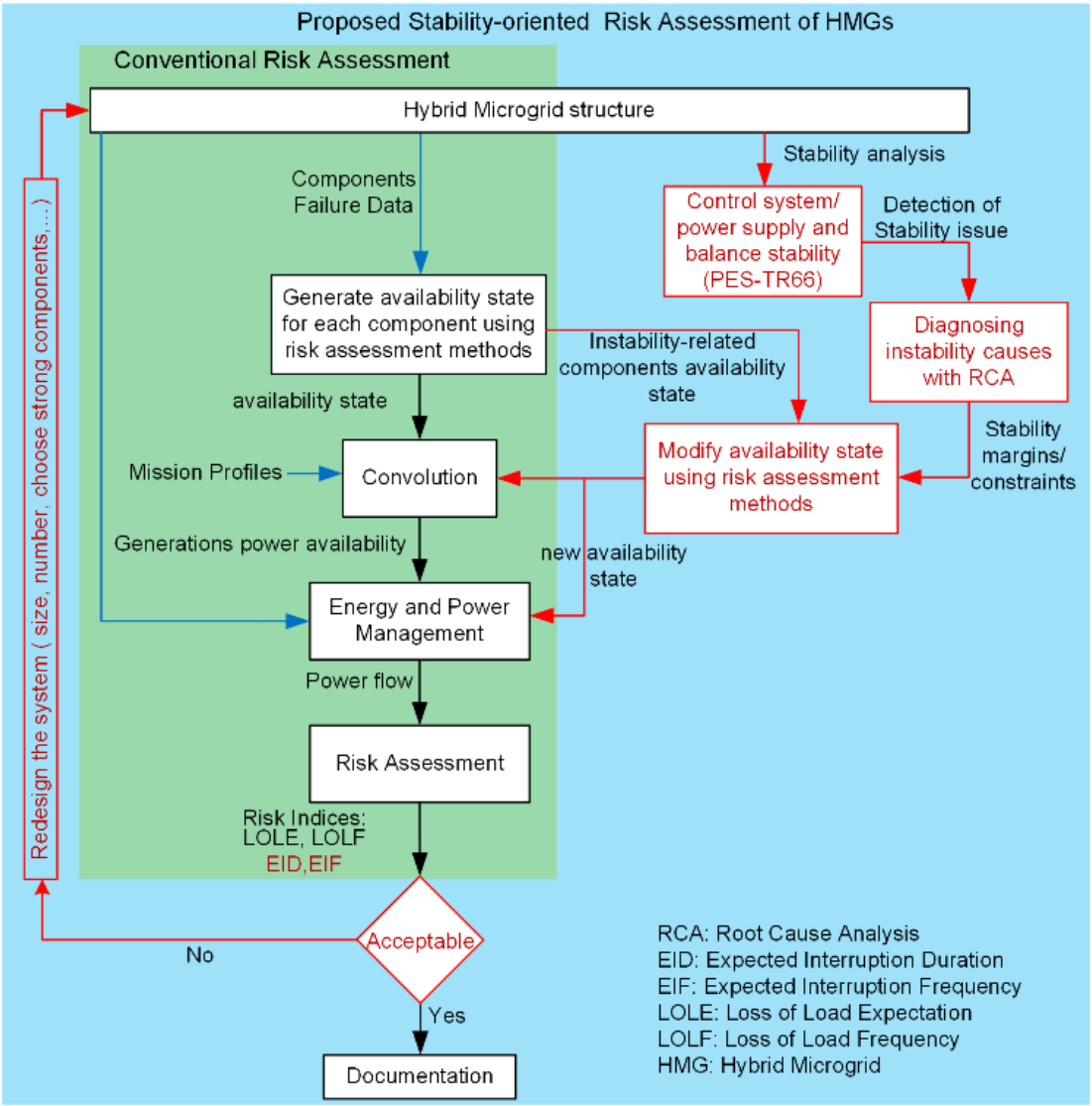

Fig. 4. *The proposed stability-oriented risk assessment model for HMGs*

Therefore, the impact of component failures on both system risk and stability can be modeled accurately. Since the proposed method considers both static and dynamic failures of the system, two new reliability indices are introduced in this study as follows:

(1) Expected Interruption Duration (EID)
(2) Expected Interruption Frequency (EIF)

The mathematical models of EID and EIF are defined in equations (18) and (19), respectively:

$$EID = LOLE + (dynamic\ performance) \quad hr/year$$
$$= \frac{1}{N}.\sum_{i=1}^{N} LLD_i + \frac{1}{N}.\sum_{j=1}^{k}\sum_{i=1}^{N} ULD_i\,(S_m^j) \tag{18}$$

$$EIF = LOLF + (dynamic\ performance) \quad occ/year$$
$$= \frac{1}{N}.\sum_{i=1}^{N} LLO_i + \frac{1}{N}.\sum_{j=1}^{k}\sum_{i=1}^{N} ULO_i\,(S_m^j) \tag{19}$$

In the above equations, k is the number of components leading to stability issues in the system, ULD_i is the unsupplied load duration resulting from stability margin (S_m), and ULO_i is the unsupplied load occurrence resulting from stability margin (S_m).

After evaluating the overall system risk, if the risk indices fall within the acceptable desired level, the design process will be completed without any further changes to the system. Otherwise, the system must be redesigned with regard to factors such as size, number of components, and selection of stronger devices.

This method provides an optimal design guideline for HMGs to comply with the acceptable desired level of system risk, taking into account both dynamic and static failures. In the next section, the proposed model will be implemented on the HMG depicted in Fig. 1, and the impact of dynamic failures, various load profiles, and IC redesign on the overall system risk will be investigated.

4. Numerical Analysis

To illustrate the impact of stability issues and the resulting dynamic failures on the overall system risk, the AC/DC hybrid microgrid shown in Fig. 1 has been considered as a test system. The DC sub-grid of the microgrid is supplied by

a 10 kW Photovoltaic (PV) system and a 10 kW Fuel Cell (FC) system, while the AC sub-grid is fed by two10 kW Microturbines (MT). In case of any power shortages, a 10 kVA Interlinking Converter (IC) connected between the AC and DC sub-grids transfers the excess power to either side as needed.

As per the proposed model, the first step towards evaluating the system risk using the new approach is to determine the stability margin for the system. Therefore, the next section will focus on performing time domain simulations to verify the small signal results obtained in Section 2 and demonstrate the impact of the IC rectifying mode of operation on the instability of DC-link voltage. Subsequently, the implications of this stability issue on the overall system risk will be discussed.

4.1. Time Domain Simulation Results

The Root locus analysis has revealed that existing a zero in the transfer function of $W(s)/I_{gd}(s)$ as shown in equation (15), leading to instability in the DC voltage of the IC when it operates in rectifying mode. To further demonstrate this instability, two case studies have been conducted in the time domain simulations, showcasing both inversion and rectifying modes of operation for the IC. The relevant parameters for the IC can be found in Table 2 of the appendices [34].

4.1.1 The IC Inversion Mode of Operation

In this case study, it is assumed that the ac sub-grid load is overloaded and there is sufficient power to transfer from dc to ac sub-grid. The load characteristics in per unit for 4-seconds timespan are shown in Table 1, considering the IC capacity as a base power ($S_b = 10\ kVA$). The dynamic responses of power and the DC-Link voltage are depicted in Fig. 5. As shown in Table 1, the dc sub-grid load is considered a constant value at 1 pu. From time t=0 to 2 s, the ac load increases from 1 to 2 pu and the ac sub-grid is capable to supply the load. At t=2 s, the ac load is overloaded to 2.5 pu. Therefore, as shown in Fig. 5 (a), the IC transfers 0.5 pu power from dc to ac side, and the DC-link voltage is stable according to the Fig. 5 (b). The ac load is also increased at t=3 and 4 s to 2.93 and 3 pu, respectively. Under these conditions, the IC successfully transfers the required power in the inversion mode without any instability in the DC-link voltage. Thus, the IC can transfer its rated capacity (10 kVA or 1 pu) and ensure the stability of the DC-link voltage while operating in the inversion mode.

4.1.2 The IC Rectifying Mode of Operation

In this case study, the impact of power transfer from ac to dc sub-grid on the stability of the DC-link voltage has been analyzed. The load in the ac sub-grid is constant at 1 pu, while the dc load varies from 1 pu to 3 pu, as shown in Table 1 for rectifying mode. The dynamic response of the generation unit, IC power flow and the DC-link voltage are shown in Fig. 6. In this case, the IC operates in rectifying mode with power flowing from the ac to dc side. As Fig. 6 (a) illustrates, for the time period from t=0 to 2 s, the dc sub-grid supplies its load up to 2 pu. At t=2 s, the dc load is increased to 2.5 pu and the IC transfers -0.5 pu excess power from the ac to the dc side. The dc load further increases to 2.93 pu at t=3 s and the IC continues to supply the required excess power from the ac side. In this condition, the DC-link voltage remains stable as depicted in Fig. 6 (b). However, when the dc load increases to 3 pu at t=4 s, the DC-link voltage becomes unstable, resulting in the HMG operating in an unstable condition.

Thus, based on the RCA demonstrated and time domain simulations, a proper stability margin needs to be defined in order to ensure the stable operation of the IC in rectifying mode. The time domain results indicate that by setting the stability margin (S_m) to 0.93, the HMG can operate in a stable condition.

Therefore, this criterion will be utilized in the risk assessment model. The next sections will describe the applied power management and energy flow strategy for the HMG illustrated in Fig. 1. Then, the risk assessment, considering various scenarios, will be modelled.

4.2. Power Management and Energy Flow

The power flow management is carried out based on the HMG's topology and generation/load limitations, as shown in Fig. 4, before executing the risk assessment and obtaining the risk indices. Following the HMG structure in Fig. 1 and the control system of the IC in Fig. 2, the power management is performed as follows:

In the dc sub-grid, the PV (G3) and Fuel Cell (G4) supply power to the dc load, while the ac load in the ac sub-grid is powered by two microturbines (G1, G2). The IC is not authorized to transfer power as long as both sub-grids can meet their respective load demands. To achieve this, the total generation (P_G) and consumption (P_L) of each side are monitored, and when P_G is equal or greater than P_L, the value of K_c in control system is set to "zero". However, in the event of power shortage ($P_G < P_L$), the IC can transfer the required power to both sides by setting an appropriate value for K_c In accordance with equation (9). The direction of power transfer is determined by the changes in V_{pu}/f_{pu}.

4.3. Impact of stability on HMG Risk

In this scenario, we investigate the impact of bridging the stability and reliability on the overall system risk. The failure data of the converters are presented in Table 3 of the appendices, where the aging of the converters is modeled using the Weibull distribution function (α and β are scale and shape factors, respectively). Additionally, the hourly load profile of Fig. 8 (a) and solar irradiance profile of Fig. 9 (a) are considered for this analysis. Fig. 7 shows the system-level risk indices for both conventional and proposed methods. Incorporating stability and dynamic failure into the system increases the overall risk of the system. For example, the risk results in Fig. 7 (a) reveal a 4.6% difference between EID and

Table 1 Load characteristics in pu during the specified time

		Time (s)				
	Load	0	1	2	3	4
Inversion mode	AC load (pu)	1	2	2.5	2.93	3
	DC load (pu)	constant= 1				
Rectifying mode	AC load (pu)	constant= 1				
	DC load (pu)	1	2	2.5	2.93	3

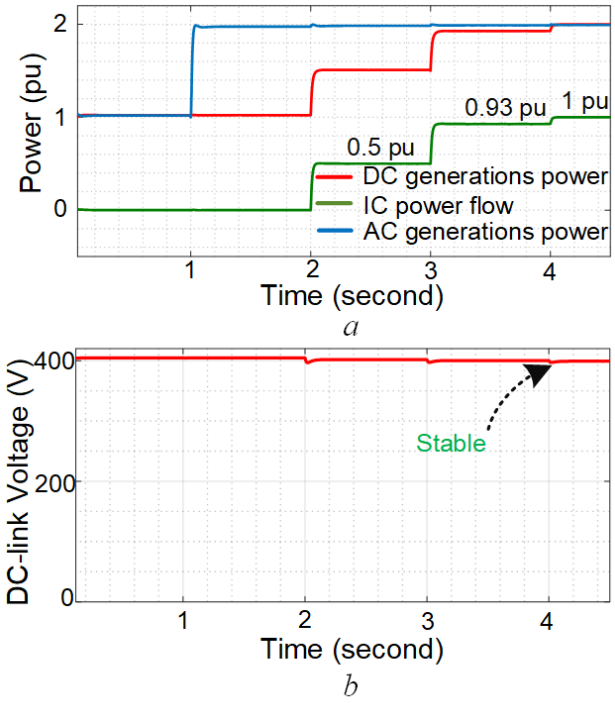

Fig. 5. *Dynamic response of DC-link voltage, power flows of dc and ac subgrids and interlinking converter power flow in inversion mode of operation,* **(a)** Power**, (b)** DC voltage

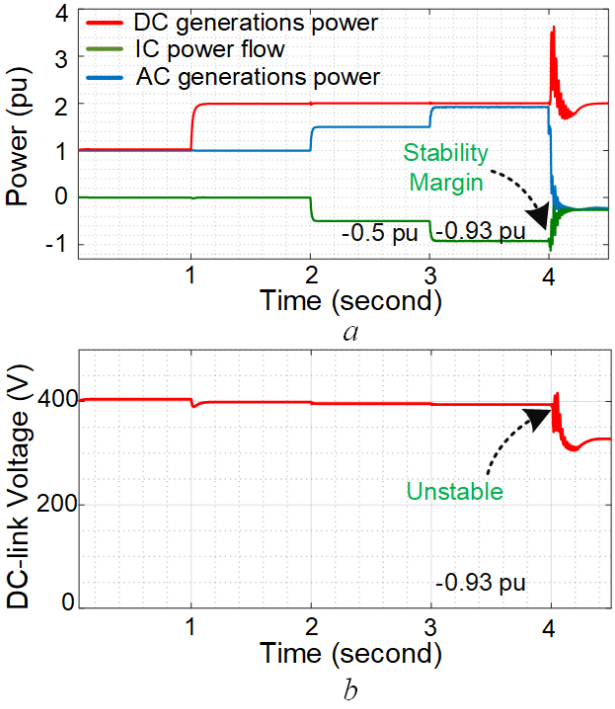

Fig. 6. *Dynamic response of DC-link voltage, power flows of dc and ac subgrids and interlinking converter power flow in rectifying mode of operation,* **(a)** Power**, (b)** DC voltage

LOLE in the first year, which grows to 18% in the 27th year. This is significant because it suggests that dynamic performance has a considerable impact on the overall system risk. These results also emphasize the strong coupling between static and dynamic failures in the system, meaning that the aging of the converters increases the risk of instability in the grid and, consequently, the risk of loss of load.

The inclusion of dynamic failure in the analysis also

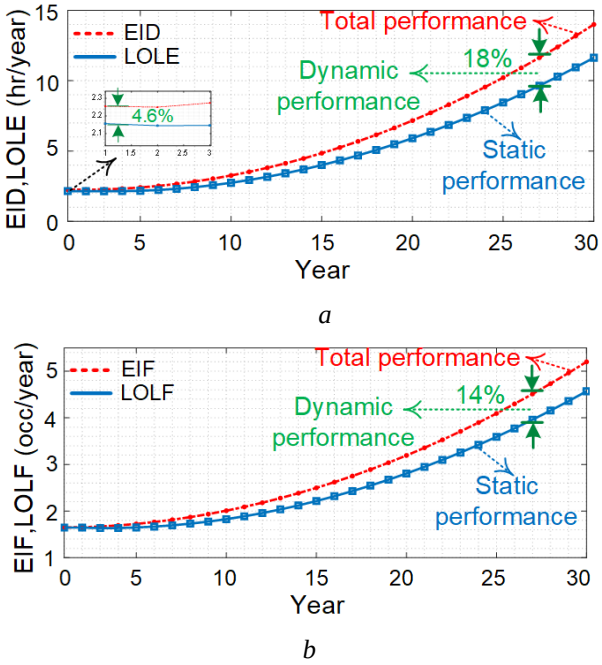

Fig. 7. *System-level risk indices for hybrid microgrid shown in Fig. 1 with/without stability margin.* **(a)** EID and LOLE**, (b)** EIF and LOLF

impacts the frequency of failures in the HMGs. Fig. 7 (b) reveals that the overall risk (EIF), which considers both static and dynamic performance, is consistently higher than the LOLF throughout the 30-year lifespan, resulting in a 14% difference in the 27th year. These findings demonstrate that the proposed model provides a more precise risk assessment when stability issues are included. However, it also highlights that the overall risk may surpass the acceptable and standard desired level of reliability for the system, necessitating the optimal redesign of the system to maintain risk within acceptable limits.

4.4. Impact of Different Load/Solar Irradiance Profiles

The risk indices are derived by combining generation and load profiles. Therefore, different load profiles will result in various risk indices, and this will be paramount in presence of stability. To illustrate the impact of different load profiles on system risk, two load profiles have been considered as Fig. 8 (a) and (b). As it can be seen, the load characteristics differ in terms of MWh and load peak distribution. For example, Fig. 8 (c) compares the cumulative distribution function (CDF) of dc loads. In 50% of the time, dc load profile 1 is higher than 11.9 kW, whereas it is 6.5 kW for dc load profile 2. This means that using dc load profile 1 will require more power flow from the IC in rectifying mode.

By employing load profiles and considering the solar irradiance profile of Fig. 9 (a), the overall risk indices are as shown in Fig. 10. As the results indicate, the overall risk related to load profile 1 for both dynamic and static performance is higher than load profile 2. Fig. 10 also shows that for some load profiles, the risk indices may vary within an acceptable level for both dynamic and static performance, and there is no need to redesign the system. For instance, considering Fig. 10 (a), even though the EID is 24% higher

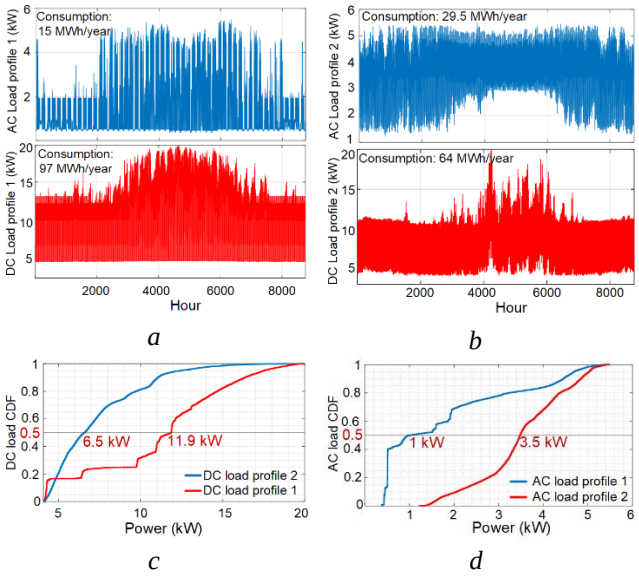

Fig. 8. *Hourly load profiles and Cumulative Distribution Function (CDF) of loads.* **(a)** Load profile 1**, (b)** Load profile 2**, (c)** CDF of DC loads**, (d)** CDF of AC loads

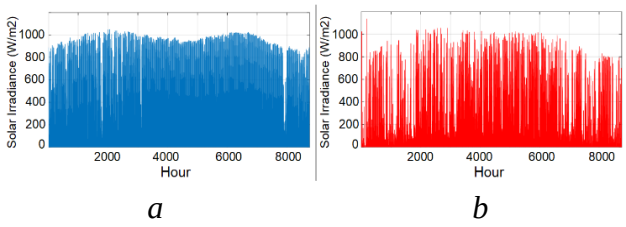

Fig. 9. *Annual solar Irradiance profiles for PV system.* **(a)** Irradiance profile 1**, (b)** Irradiance profile 2

than LOLE for load profile 2 in the 27th year, the overall risk at the end of system's lifetime is significantly lower than the risks associated with load profile 1. There is around 55% reduction in EID, indicating that the risk results of load profile 2 may vary within standard margins, and for the HMG with this type of load, there is no need for further optimal design.

Another important point to consider is that dynamic failure may have worst impact on system risk, even if the total risk has decreased. According to Fig. 10 (b), the EIF is 27% higher than LOLF for load profile 2, while this value is only 14% for load profile 1 which has higher overall risk. This is mainly due to the existence of more peak loads on the dc side for load profile 2, requiring the IC to transfer more power in rectifying mode. However, the stability margin confines the flow of power, leading to an increase in the loss of load due to the dynamic performance and ultimately resulting in a higher risk in the system.

These results confirm that load characteristics have a significant impact on the overall system risk, especially when it comes to dynamic failures. However, in some cases, they may guarantee the desired standard level of risk, and there is no need to redesign the system.

Additionally, the non-dispatchable sources and their various mission profiles play a critical role in the total performance and reliability of a system. As depicted in Fig. 11, a comparison of the HMG risk for the solar irradiance profiles shown in Fig. 9 (a) and (b) reveals crucial insights. According to Fig. 11 (a), reduced solar energy availability during periods of low irradiance (e.g., irradiance profile 2) leads to a higher risk for the system. For example, the EID and LOLE increase by 19% and 17%, respectively. Notably, the impact of changing the solar irradiance profile on EIF/LOLF, as illustrated in Fig. 11 (b), is even more significant, resulting in an approximately 50% higher risk compared to the results obtained from irradiance profile 1. This emphasizes the importance of considering uncertainties coming from different solar irradiance profiles as distinct generation sources in the design and evaluation of the system risk.

4.5. Impact of Different ICs Structure

As outlined in the proposed model, after obtaining the new risk indices, which takes into account both static and dynamic failures, the system risk indices may not be in an acceptable level. If this occurs, different scenarios can be considered to redesign the system while consider stability and reliability perspectives based on the structure of the HMG. The key advantage of the proposed model is that the redesign process is carried out with a holistic approach that considers both perspectives. In this case study, the 10 kVA IC was replaced with two 5 kVA ICs using the same failure data. Fig. 12 illustrates the configuration of the ICs, which are connected between ac and dc sub-grid. Fig. 13 compares the system-level risk indices for the aforementioned structures. According to Fig. *13* (a), using two ICs with the same total capacity results in an 18% reduction in EID and 21% in LOLE compared to using a single 10 kVA IC.

This reconfiguration also affects the number of failures, as shown in Fig. 13 (b). The reduction in EIF is 7%, and for LOLF, it is 9% compared to the single IC connection.

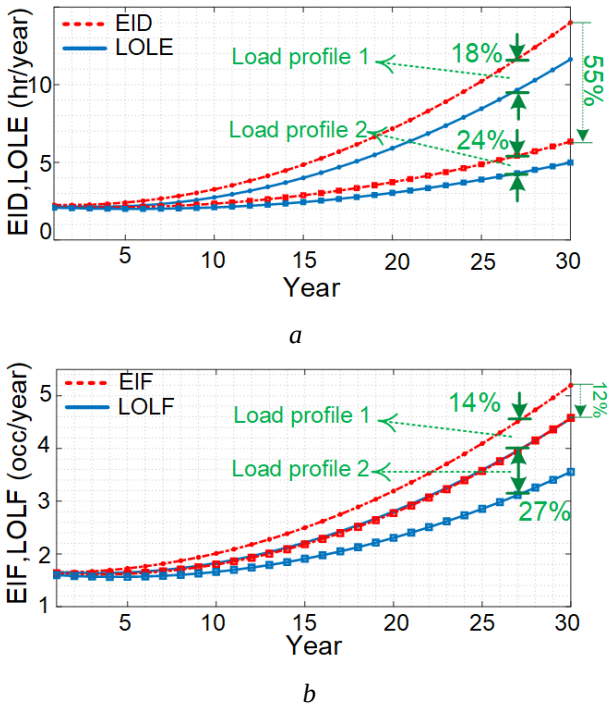

Fig. 10. *System-level risk indices for load profile 1 (dot marker) and load profile 2 (square marker) considering the solar irradiance profile 1 shown in Fig. 9 (a).* **(a)** EID and LOLE, **(b)** EIF and LOLF

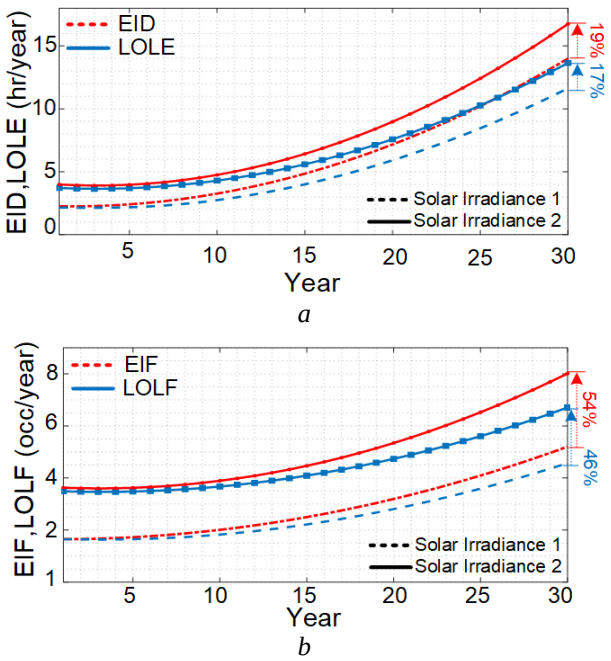

Fig. 11. *System-level risk indices for solar irradiance 1 (dash lines) and solar irradiance 2 (solid lines) considering load profile 1 characteristics.* **(a)** EID and LOLE**, (b)** EIF and LOLF

In fact, increasing the number of ICs provides the system with the opportunity to avoid losing all the power flow in case of IC failure. When only one IC is present in the system, failure results in the loss of the entire 10 kVA capacity. However, with two ICs, if one fails, the other can still transfer power up to 5 kVA.

Although this approach shows promising results, there is still a significant difference between dynamic and static performance. Therefore, it is recommended for systems where the overall risk is not excessively high (e.g., load profile 2) and we need to reduce the risk by 10-20% to ensure acceptable system performance.

To manage and reduce the impact of dynamic performance, other approaches can be used, such as redesigning the converter that has the dominant impact on dynamic performance, optimal oversizing of IC, changing the number of ICs with different capacities, and adding more renewable sources to the DC side. However, all these approaches require an exact sensitivity analysis, which will be conducted in future works.

5. Conclusion

This paper presents a modelling approach that connects stability and reliability to ensure overall risk in HMGs. The proposed method highlights the significant impact of dynamic failures on overall system risk, in addition to the static failures that comes from component failures. Furthermore, the results underscore the interplay between dynamic and static failures, as the aging of converters can lead to system instability and an increased risk of load loss.

The results also indicate that the AC/DC load profiles have a significant impact on the system risk. For certain load profiles, the risk indices, considering the stability margins, may fall within acceptable levels. However, in some cases,

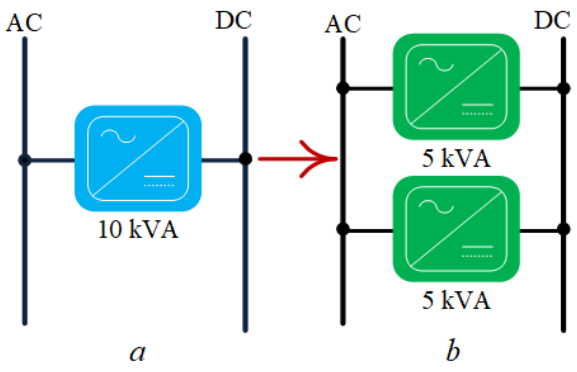

Fig. 12. *A hybrid microgrid with* ***(a)*** a single 10 kVA IC, *and* ***(b)*** two 5 kVA ICs

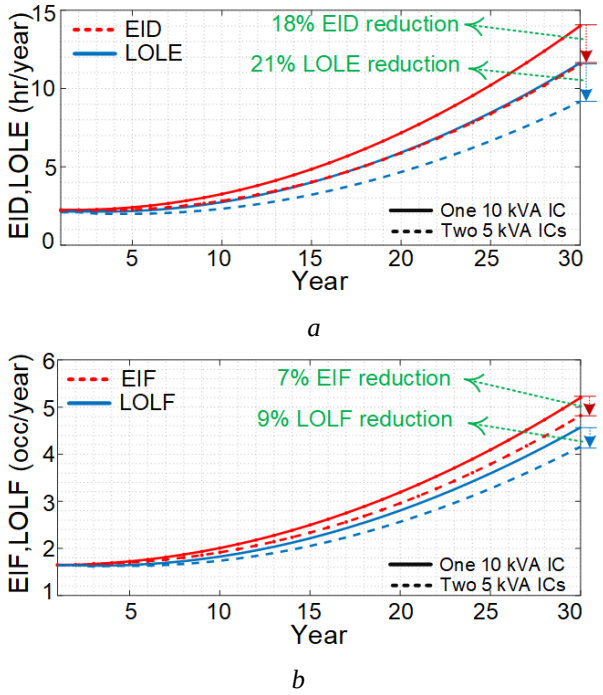

Fig. 13. *System-level risk indices for different IC structures: one 10 kVA IC (solid) and two 5 kVA ICs (dashed)*
(a) EID and LOLE, **(b)** EIF and LOLF

the load characteristics may lead to an increase in overall risk and a deterioration of dynamic performance. Thus, load profiles are a crucial factor in HMG design.

In addition to its ability to provide an optimal and comprehensive guideline for system redesign or reconfiguration, the proposed method demonstrated that increasing the number of interlinking converters with the same total capacity can significantly reduce the risk of the system, despite the persistence of dynamic failures, which contribute to increased total risk. This reconfiguration method is suitable for systems requiring only a small reduction in risk to ensure a stable and reliable operation.

This model simplifies the coupling of system risk with the stability and reliability of the HMG. Therefore, optimized design and sizing of the components can be achieved to ensure an acceptable system performance.

The future investigation will focus on optimal design and operation of HMGs considering multiple generation sources and interlinking converters in terms of number and capacity.

6. Appendices

Table 2 The characteristics and settings of the interlinking converter and its control system

Symbol	Simulation
V_{dc} (V)	400
f_0 (Hz)	50
V_{dc}^{min}, V_{dc}^{max} (V)	390,410
K_c	8000
f^{min}, f^{max} (Hz)	49,51
L_f (mH)	4.5
k_p, k_I	8,120
$k_{p.PLL}$, $k_{I,PLL}$	40,1000

Table 3 Failure data of hybrid microgrid converters

Definition	Failure rate	Repair rate	Weibull distribution factors	
	λ (10^{-6}f/hr)	μ (r/hr)	α (yr)	β
Interlinking Converter	2.2	0.007	20	3.8
PV	2.9	0.01	22	4
Microturbine	1.2	0.0125	22	3.5
Fuel Cell	2.1	0.0083	19	3.42

7. References

[1] Jiménez-Vargas, I., Rey, J.M., Osma-Pinto, G.: 'Sizing of hybrid microgrids considering life cycle assessment', Renewable Energy, 2023, 202, pp. 554–565.

[2] Saeed, M.H., Fangzong, W., Kalwar, B.A., Iqbal, S.: 'A Review on Microgrids' Challenges & Perspectives', IEEE Access, 2021, 9, pp. 166502–166517.

[3] Muyeen, S.M., Islam, S.M., Blaabjerg, F.: 'Variability, scalability and stability of microgrids', (Institution of Engineering and Technology, 2019)

[4] Peyghami, S., Wang, Z., Blaabjerg, F.: 'A Guideline for Reliability Prediction in Power Electronic Converters', IEEE Trans. Power Electron., 2020, 35, (10), pp. 10958–10968.

[5] Peyghami, S., Blaabjerg, F.: 'Demands for Bridging Power Electronics and Power System Engineering Concepts', in '2020 5th IEEE Workshop on the Electronic Grid (eGRID)' (ieeexplore.ieee.org, 2020), pp. 1–8

[6] Eshkaftaki, A.A., Rabiee, A., Kargar, A., Boroujeni, S.T.: 'An Applicable Method to Improve Transient and Dynamic Performance of Power System Equipped With DFIG-Based Wind Turbines', IEEE Trans. Power Syst., 2020, 35, (3), pp. 2351–2361.

[7] Hoke, A., Gevorgian, V., Shah, S., Koralewicz, P., Kenyon, R.W., Kroposki, B.: 'Island Power Systems With High Levels of Inverter-Based Resources: Stability and Reliability Challenges', IEEE Electrification Magazine, 2021, 9, (1), pp. 74–91.

[8] Kundur, P.S., Malik, O.P.: 'Power system stability and control', (McGraw-Hill Education, 2022)

[9] Puschkarsky, K., Grasser, T., Aichinger, T., Gustin, W., Reisinger, H.: 'Review on SiC MOSFETs High-Voltage Device Reliability Focusing on Threshold Voltage Instability', IEEE Trans. Electron Devices, 2019, 66, (11), pp. 4604–4616.

[10] Barón, K.M., Sharma, K., Nitzsche, M., Kallfass, I.: 'Online Monitoring of Degradation Sensitive Electrical Parameters in Inverter Operation for SiC-MOSFETs', in '2021 IEEE Applied Power Electronics Conference and Exposition (APEC)' (ieeexplore.ieee.org, 2021), pp. 1235–1241

[11] Firdaus, A., Mishra, S.: 'Mitigation of Power and Frequency Instability to Improve Load Sharing Among Distributed Inverters in Microgrid Systems', IEEE Syst. J., 2020, 14, (1), pp. 1024–1033.

[12] Wang, X., Blaabjerg, F.: 'Harmonic Stability in Power Electronic-Based Power Systems: Concept, Modeling, and Analysis', IEEE Trans. Smart Grid, 2019, 10, (3), pp. 2858–2870.

[13] Peyghami, S., Palensky, P., Blaabjerg, F.: 'An Overview on the Reliability of Modern Power Electronic Based Power Systems', IEEE Open Journal of Power Electronics, 2020, 1, pp. 34–50.

[14] Li, W.: 'Risk Assessment of Power Systems: Models, Methods, and Applications' (John Wiley & Sons, 2014)

[15] Ahsan, M., Hon, S.T., Batunlu, C., Albarbar, A.: 'Reliability Assessment of IGBT Through Modelling and Experimental Testing', IEEE Access, 2020, 8, pp. 39561–39573.

[16] Yao, B., Ge, X., Wang, H., Wang, H., Zhou, D., Gou, B.: 'Multitimescale Reliability Evaluation of DC-Link Capacitor Banks in Metro Traction Drive System', IEEE Transactions on Transportation Electrification, 2020, 6, (1), pp. 213–227.

[17] Uddin Ahmed, K.M., Alvarez, M., Bollen, M.H.J.: 'Characterizing Failure and Repair Time of Servers in a Hyper-scale Data Center', in '2020 IEEE PES Innovative Smart Grid Technologies Europe (ISGT-Europe)' (ieeexplore.ieee.org, 2020), pp. 660–664

[18] Zhang, Y., Wang, H., Wang, Z., Blaabjerg, F., Saeedifard, M.: 'Mission Profile-Based System-Level Reliability Prediction Method for Modular Multilevel Converters', IEEE Trans. Power Electron., 2020, 35, (7), pp. 6916–6930.

[19] Xiao, Y., Zhang, Z., Duraij, M.S., Zsurzsan, T.-G., Andersen, M.A.E.: 'Review of High-Temperature Power Electronics Converters', IEEE Trans. Power Electron., 2022, 37, (12), pp. 14831–14849.

[20] Fischer, K., Steffes, M., Pelka, K., Tegtmeier, B., Dörenkämper, M.: 'Humidity in Power Converters of Wind Turbines—Field Conditions and Their Relation with Failures', Energies, 2021, 14, (7), p. 1919.

[21] Samavatian, V., Fotuhi-Firuzabad, M., Dehghanian, P., Blaabjerg, F.: 'Reliability Modeling of Multistate Degraded Power Electronic Converters With Simultaneous Exposure to Dependent Competing Failure Processes', IEEE Access, 2021, 9, pp. 67096–67108.

[22] Ge, S., Sun, H., Liu, H., Li, J., Zhang, X., Cao, Y.: 'Reliability Evaluation of Multi-energy Microgrids: Energy Storage Devices Effects Analysis', Energy Procedia, 2019, 158, pp. 4453–4458.

[23] Khare, V., Nema, S., Baredar, P.: 'Reliability analysis of hybrid renewable energy system by fault tree analysis', Energy Environ., 2019, 30, (3), pp. 542–555.

[24] Marvin Rausand, Rausand, M., Anne Barros, Barros, A., Arnljot Hoyland, Hoyland, A.: 'System Reliability Theory: Models, Statistical Methods, and Applications' (2020)

[25] Qi, N., Cheng, L., Jiang, Y., et al.: 'Vulnerability Assessment Based on Operational Reliability Weighted and

Preventive Planning', in '2019 IEEE Sustainable Power and Energy Conference (iSPEC)' (ieeexplore.ieee.org, 2019), pp. 1749–1754
[26] Farrokhabadi, M., Cañizares, C.A., Simpson-Porco, J.W., et al.: 'Microgrid Stability Definitions, Analysis, and Examples', IEEE Trans. Power Syst., 2020, 35, (1), pp. 13–29.
[27] Yazdani, A., Iravani, R.: 'An accurate model for the DC-side voltage control of the neutral point diode clamped converter', IEEE Trans. Power Delivery, 2006, 21, (1), pp. 185–193.
[28] Yazdani, A., Iravani, R.: 'Voltage-sourced converters in power systems: modeling, control, and applications', John Wiley & Sons, 2010, Chapter 8.
[29] Eajal, A.A., Muda, H., Aderibole, A., Hosani, M.A., Zeineldin, H., El-Saadany, E.F.: 'Stability Evaluation of AC/DC Hybrid Microgrids Considering Bidirectional Power Flow Through the Interlinking Converters', IEEE Access, 2021, 9, pp. 43876–43888.
[30] Hajiakbari Fini, M., Hamedani Golshan, M.E.: 'Determining optimal virtual inertia and frequency control parameters to preserve the frequency stability in islanded microgrids with high penetration of renewables', Electric Power Syst. Res., 2018, 154, pp. 13–22.
[31] Ali, H., Magdy, G., Xu, D.: 'A new optimal robust controller for frequency stability of interconnected hybrid microgrids considering non-inertia sources and uncertainties', Int. J. Electr. Power Energy Syst., 2021, 128, p. 106651.
[32] Wang, R., Sun, Q., Ma, D., Liu, Z.: 'The Small-Signal Stability Analysis of the Droop-Controlled Converter in Electromagnetic Timescale', IEEE Transactions on Sustainable Energy, 2019, 10, (3), pp. 1459–1469.
[33] Hatziargyriou, N., Milanovic, J., Rahmann, C., et al.: 'Definition and Classification of Power System Stability – Revisited & Extended', IEEE Trans. Power Syst., 2021, 36, (4), pp. 3271–3281.
[34] Peyghami, S., Mokhtari, H., Blaabjerg, F.: 'Autonomous Operation of a Hybrid AC/DC Microgrid With Multiple Interlinking Converters', IEEE Trans. Smart Grid, 2018, 9, (6), pp. 6480–6488.
[35] Billinton, Li, W.: 'Reliability Assessment of Electric Power Systems Using Monte Carlo Methods' (Springer Science & Business Media, 2013)
[36] Wang, X., Zhao, X., Wang, S., Sun, L.: 'Reliability and maintenance for performance-balanced systems operating in a shock environment', Reliab. Eng. Syst. Saf., 2020, 195, p. 106705.
[37] Bilal, M., Rizwan, M., Alsaidan, I., Almasoudi, F.M.: 'AI-Based Approach for Optimal Placement of EVCS and DG With Reliability Analysis', IEEE Access, 2021, 9, pp. 154204–154224.
[38] Allan, R.N., Billinton: 'Reliability Evaluation of Power Systems' (Springer Science & Business Media, 2013)